Phthalocyanine-polyoxotungstate lanthanide double deckers

COMMUNICATION

Phthalocyanine-Polyoxotungstate Lanthanide Double Deckers

Sidra Sarwar,[a,b] Sergio Sanz,[b,c] Jan van Leusen,[a] Gary S. Nichol,[d] Euan K. Brechin*[d] and Paul Kögerler*[a,b,c]

Received 00th January 20xx,
Accepted 00th January 20xx

DOI: 10.1039/x0xx00000x

Acetate ligand metathesis results in the first hybrid $[M^{III}(Pc)(PW_{11}O_{39})]^{6-}$ (M = Y, Dy, Tb) double-decker scaffolds, where a phthalocyanate (Pc^{2-}) and one of the conceptually most simple polyoxotungstates, a monolacunary Keggin cluster, are interlinked via a single rare earth ion. Characterisation included high-resolution mass spectrometry, synchrotron-based single-crystal X-ray diffraction, various spectroscopic and electrochemical methods, and magnetic studies revealing slow relaxation of the magnetisation for the Dy derivate.

Single-molecule magnets (SMMs), characterised by magnetic bi-stability due to a finite spin ground state and a negative axial zero-field ground state splitting,[1,2] continue to raise interest in the context of quantum computation and molecular spintronics.[3-9] Here, rare earth spin centres are specifically targeted due to their large intrinsic magnetic anisotropy arising from the near degeneracy of the 4*f* orbitals.[10,11] They offer a key advantage in that and, through careful ligand field design, it is possible to manipulate the magnitude and alignment of anisotropy axes.[12-14] Following this strategy, sandwich-type complexes based on late rare earth metals with phthalocyanine (and other high-symmetry aromatic) ligands have shown great promise as SMM architectures by harnessing 4*f* single-ion anisotropy.[15-19] The synthesis of homoleptic and heteroleptic double-decker complexes with phthalocyanine ligands has been extensively explored, with significant changes observed in magnetic properties upon chemical modification of peripheral substituents.[20-25] To a lesser extent, synthetic chemists have explored replacing one of the phthalocyanine ligands with a polydentate ligand to impose structural changes associated with the chemical and physical properties of the new ligands. Examples include Schiff bases, porphyrins and organometallic tripodal ligands.[26-33] Note that even the replacement of some pyrrole units in the macrocyclic framework with e.g. furan or thiophene, result in a significant change in the magnetic characteristics.[34] On the other hand, redox-active lacunary polyoxometalates act as versatile polydentate ligands towards oxophilic lanthanide ions, resulting in application potentials in electrochemistry, photochemistry, catalysis and magnetism.[35-45] Despite these prospects, there is just one report of a double-decker Ln^{III} complex comprising both a phthalocyanine and a polyoxometalate, namely a Yb^{3+} complex with a polyoxovanadate.[46] In contrast, we here focus on the lanthanide ions Tb^{3+} ($4f^8$) and Dy^{3+} ($4f^9$) that exhibit especially high magnetic anisotropy in $LnPc_2$-type double decker complexes,[15] in conjunction with a thermodynamically highly stable, classical polyoxotungstate ligand.

Herein, we describe the synthesis and characterisation of a new class of Ln double-decker species isolated as $(N(nBu)_4)_4H_2[M^{III}Pc(PW_{11}O_{39})]$ with M = Y (**1**), Dy (**2**) or Tb (**3**) that contain a Pc^{2-} and a monolacunary α-Keggin ($[P^{V}W^{VI}_{11}O_{39}]^{7-}$) ligand. Key to these syntheses is the precursor [M(Pc)(OAc)], which is reacted with $(N(nBu)_4)_4H_3[PW_{11}O_{39}]$, $N(nBu)_4Br$ and NEt_3 in a 1:1:1 mixture of CH_3CN:MeOH:CH_2Cl_2 overnight at 50 °C. The resulting solution is filtered and the mother liquor evaporated to dryness. Precipitation of the dissolved crude material in CH_2Cl_2 with hexane renders a green powder, which is purified by column chromatography. We started with the diamagnetic analogue, $[Y^{III}(Pc)(PW_{11}O_{39})]^{6-}$, to examine its solution behaviour *via* ^1H and ^{31}P NMR. Thereafter, **2** and **3** were isolated from similar synthetic procedures, with green rod-like crystals of **3** grown through slow evaporation of a CH_2Cl_2 solution.

The ^1H NMR (600 MHz, CD_3CN) spectrum of $[Y^{III}(Pc)(PW_{11}O_{39})]^{6-}$ presents broad singlets for H_α (9.61–9.20 ppm) and H_β (8.34–8.05 ppm) of the Pc ligand, characteristic of a reduced symmetry in the complex (Figure S12). While a shift of H_α from ca. 9.42 to 9.50 ppm is observed when the single-decker phthalocyanate complex [YPc(OAc)] coordinates to $[PW_{11}O_{39}]^{7-}$, H_β remains relatively unchanged. The ^{31}P NMR (243 MHz, CD_3CN) spectrum shows a shift from –13.24 to –14.64 ppm of the $[PW_{11}O_{39}]^{7-}$

[a] *Institute of Inorganic Chemistry, RWTH Aachen University, 52056 Aachen, Germany.*
[b] *Peter Grünberg Institute, Electronic Properties (PGI-6), Forschungszentrum Jülich, 52425 Jülich, Germany.*
[c] *Jülich-Aachen Research Alliance, Fundamentals for Future Information Technology (JARA-FIT), Forschungszentrum Jülich, 52425 Jülich, Germany.*
[d] *EaStCHEM School of Chemistry, The University of Edinburgh, David Brewster Road, Edinburgh, EH9 3FJ, UK*

Electronic Supplementary Information (ESI) available: Synthetic description, characterisation and additional figures related to the discussion of results. See DOI: 10.1039/x0xx00000x

precursor (Figures S10, S13). NMR, EA, IR, UV-Vis, and ESI HRMS are consistent with the purity of the diamagnetic analogue and support the existence of the counteraction composition in **1**. Subsequently, compounds **2** and **3** were synthesised and characterised by ESI-HRMS, IR, UV-Vis, and EA. Akin to the Y complex (see SI for crystallography information), green rod-like crystals of **3** were obtained from a concentrated CH_2Cl_2 solution. Several attempts to obtain single crystals of **2** using different mixtures of solvents, cation exchange and crystallisation conditions failed. Both **1** and **3** crystallise in a monoclinic system and structure solution was performed in the $P2_1/c$ and $C2/m$ space groups, respectively. The molecular {$MPc(PW_{11}O_{39})$} units in **1** and **3** are virtually isostructural, and in the following we discuss the representative structure **3**. $[PW_{11}O_{39}]^{7-}$, the monolacunary derivative of the seminal α-Keggin-type polyanion $[PW_{12}O_{40}]^{3-}$, contains a central phosphate (P–O: 1.478–1.547 Å), coordinating to 11 W^{VI} ions via three μ_3-O and one μ_2-O_P sites (W–O: 2.390–2.498 Å). On the periphery, the W^{VI} ions are linked by μ_2-O^{2-} ions (W–O: 1.792–2.077 Å), with the remaining coordination sites completed by terminal oxo groups (W–O: 1.684–1.704 Å). The defect (lacuna) site of $[PW_{11}O_{39}]^{7-}$ is defined by four basic oxygen atoms (O···O: 2.81–2.94 Å) that coordinate to the TbPc unit and generate $[Tb^{III}(Pc)(PW_{11}O_{39})]^{6-}$ with Tb^{III} adopting a distorted square-antiprismatic N_4O_4 environment (Tb–O: 2.361 and 2.389 Å; Tb–N: 2.452, 2.465 and 2.467 Å). The TbN_4O_4 fragment is rotated by a skew angle of 46.08° and 44.44° relative to an eclipsed geometry. The symmetry plane of the C_s-symmetric {PW_{11}} unit approximately aligns with one of the two σ_v planes of the Pc unit (Figure 1). This effectively tilts the Pc group to one side, hence breaking the equivalency of pyrrolic units, in line with the low symmetry observed by NMR of the Y derivative.

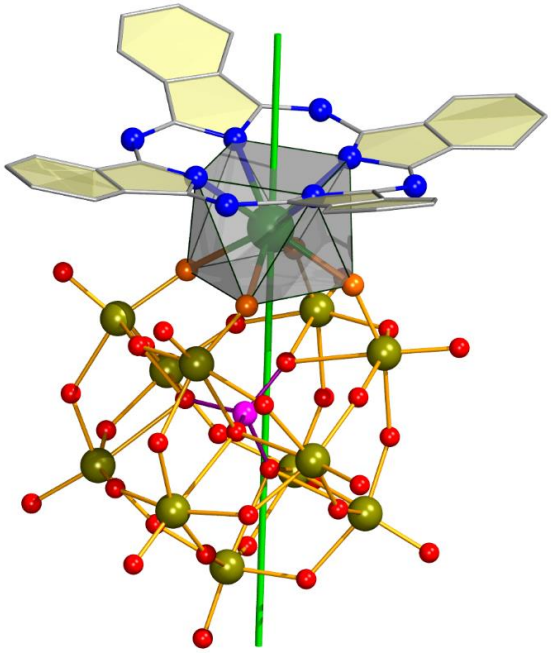

Figure 1. Molecular structure of the $[Y^{III}(Pc)(PW_{11}O_{39})]^{6-}$anion in **1**. The distorted square-antiprismatic YN_4O_4 coordination polyhedron is highlighted in transparent grey, and the orientation of its associated local C_4 axis is shown as green line. The four oxygen centres surrounding the lacunary site of the $[PW_{11}O_{39}]^{7-}$ group, to which the Y^{3+} ion coordinates, are shown in orange. Colour code: Y: green, W: dark yellow, P: purple, O: red, N: blue, C: light grey. H atoms omitted for clarity. Benzene and pyrrole rings of the Pc ligand are shown in transparent yellow to better illustrate the bent Pc geometry.

The electronic absorption spectra of **1**, **2** and **3** in CH_2Cl_2 exhibit a typical Soret band at ~352 nm and an intense Q-band at ~693 and ~710 nm (Figure S8). This splitting of the Q-band, similar to other heteroleptic bis(phthalocyanato) Ln^{III} complexes, arises due to lowered molecular symmetry resulting in different possible transitions.[20,47-49] In addition to the Soret and Q-bands of Pc ligand origin, the spectra display another band at ~260 nm corresponding to an O→W charge transfer transition in the $PW_{11}O_{39}$ unit. FT-IR spectra of **1**, **2** and **3** (Figures S6, S7) display vibrations related to ν(C-H) ~2960-2853 cm^{-1}, ν(C=N) ~1632 cm^{-1}, δ(CH_2) ~1458 cm^{-1}, ν(P-O) ~1094 and 1056 cm^{-1}, ν(W-$O_{terminal}$) ~953 cm^{-1}, ν(W-O_b-W) ~886 cm^{-1} (bridging oxygen of two octahedral W sharing a corner) and ν(W-O_c-W) 800–730 cm^{-1} (bridging oxygen of two octahedral W sharing an edge). ESI-HRMS in the negative mode for **1**, **2** and **3** show fragmentations characteristic for the triply negatively charged species [M + NBu_4 +2H]$^{3-}$ and [M + 2NBu_4 + H]$^{3-}$, where M = $[Ln^{III}(Pc)(PW_{11}O_{39})]^{6-}$. The isotopic distributions of the calculated species perfectly match with *m/z* deviations within ~0.0005 and ~0.0004, respectively (Figures 2b, S4 and S5).

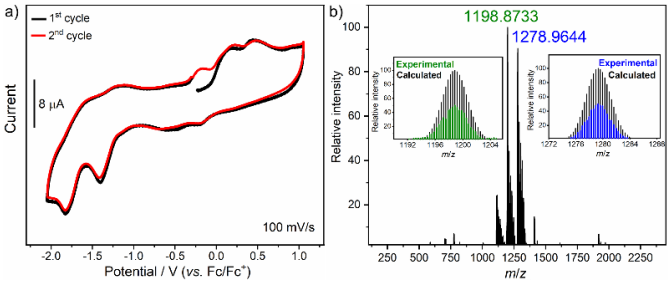

Figure 2. a) Cyclic voltammogram of a 0.33 mM solution of **2** in 0.1 M NBu_4PF_6 in CH_2Cl_2. Sweeping direction is from negative to positive potentials. b) Full ESI-HRMS spectrum of **2**, M = $[Dy^{III}(Pc)(PW_{11}O_{39})]^{6-}$. The inset shows the partial ESI-HRMS corresponding to [M + NBu_4 + 2H]$^{3-}$ = $[C_{48}H_{54}N_9O_{39}PW_{11}Dy]^{3-}$ (green) and [M + 2NBu_4 + H]$^{3-}$ = $[C_{64}H_{89}N_{10}O_{39}PW_{11}Dy]^{3-}$ (blue), compared to calculated isotopic distribution (black), corresponding to *m/z* = 1198.8732 and 1278.9649, respectively. Experimental and theoretical relative abundances have been adjusted to 50% and 100%, respectively, for the purpose of comparison.

Cyclic voltammograms of **1**, **2** and **3** were performed in 10 mL CH_2Cl_2 solutions using [NBu_4][PF_6] (0.1 M) as electrolyte, a glassy carbon working electrode, and a Pt wire as reference and counter electrode. All complexes show similar behaviour (Figures 2a and S3). Plotted data were corrected for ohmic drop (PEIS method) and referenced *vs.* $[Cp_2Fe]/[Cp_2Fe]^+$. The CVs do not display any marked redox couples, and except for the reduction potentials at E_{pc} ~ –1.80 V and E_{pc} ~ –1.40 V, the oxidation and reduction processes are not well defined. Electrochemistry of complexes containing Pc ligands show multiple redox couples based on oxidation and reduction of the Pc ring.[50-52] The $[PW_{11}O_{39}]^{7-}$ constituent is only redox-active at negative potentials showing a quasi-reversible couple W^{VI}/W^{V} at $E_{1/2}$ = –1.18 V (Figure S2). Therefore, by comparison with the starting materials, oxidation peaks at ~ –1.58, ~ +0.18 and ~ +0.46 V and reduction peaks at ~ –1.80 V are associated to Pc. Meanwhile, the observed E_{pc} ~ –1.40 V and E_{pa} ~ –1.20 V are likely overlapping redox processes occurring in both the Pc ligand and POM unit. Narrowing the window of the sweeping potential in the negative (–2.10 V to –0.24 V) and positive (–0.25 V to +0.94 V) ranges yielded identical features to the full spectra (Figure S1). Thermogravimetric analysis (TGA) of **1**, **2** and **3** (Figure S9) exhibit thermal stability until 200 °C, and up to ca. 400 °C the complexes lose all NBu_4 countercations (ca. 22 %).

Direct current (dc) magnetic susceptibility and magnetisation data for **2** and **3** are shown in Figure 3a as $\chi_m T$ vs. T at 0.1 T and M_m vs. B at 2.0 K. At 290 K, the $\chi_m T$ values are 13.26 (**2**) and 11.84 cm^3 K mol^{-1} (**3**), in good agreement with those expected for an isolated Dy^{III} or Tb^{III} centre (Dy^{III}: 13.01–14.05 cm^3 K mol^{-1}, Tb^{III}: 11.76–12.01 cm^3 K mol^{-1}).[53] Upon cooling, the values of $\chi_m T$ gradually decrease to 12.63 (**2**) or 11.24 cm^3 K mol^{-1} (**3**) at 90 K, and subsequently drop to reach 9.10 (**2**) or 9.31 cm^3 K mol^{-1} (**3**) at 2.0 K. These drop-offs are due to the thermal depopulation of the energy states of the respective split ground terms $^6H_{15/2}$ (Dy^{III}) or $^7F_6$ (Tb^{III}). At 2.0 K, the molar magnetisation as a function of the applied magnetic field (Figure 3a, inset) steeply rises at low fields (0–1 T) and slightly increases at higher fields reaching a value of 5.1 (**2**) or 4.8 $N_A\mu_B$ (**3**) at 5.0 T. As expected, this value is about half of the saturation value of a single Dy^{III} (10 $N_A\mu_B$) or Tb^{III} (9 $N_A\mu_B$) centre, since these data represent the mean value of a statistical arrangement (*i.e.* powder sample) of magnetically anisotropic lanthanide centres.

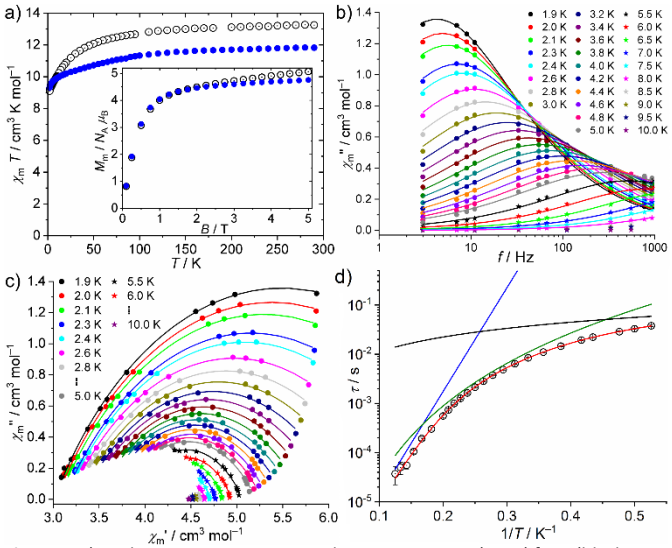

Figure 3. a) Dc data: $\chi_m T$ vs. T at 0.1 T and M_m vs. B at 2.0 K (inset) for **2** (black open circles) and **3** (blue full circles; because of the loss of lattice solvent during the treatment of the sample, leading to uncertainty in the molar mass, the $\chi_m T$ at 290 K was scaled to 11.84 cm^3 K mol^{-1}). b) out-of-phase molar magnetic susceptibility χ_m'' vs. f for **2** (symbols: data, lines: fits to generalised Debye expression). c) Magnetic ac data for **2**: Cole-Cole plot in the range 1.9–10.0 K at a static bias field of 500 Oe (symbols: data, lines: fits to a generalised Debye expression). d) Arrhenius plot of relaxation time τ vs. T^{-1} (1.9 K ≤ T ≤ 8.0 K) for **2**, red line shows a combined fit to Orbach (blue), Raman (green) and direct relaxation (black) processes.

For **3**, weak out-of-phase ac susceptibility signals were detected at static bias fields above 100 Oe and below 1000 Oe. However, the curvature in the Cole-Cole plots (Figure S16, bottom) are not pronounced enough to obtain a reliable fit. For **2**, weak out-of-phase signals were detected at zero static bias field (Figure S16, top-left). At a 500 Oe static bias field, optimal conditions for fitting the data were found, *i.e.* pronounced curvatures in the Cole-Cole plot (Figure 3c) and maxima in the χ_m'' vs. f representation (Figure 3b). The data were analysed in terms of a generalised Debye expression[54] at each temperature yielding the lines in the Cole-Cole plot and (χ_m', χ_m'') vs. f plots, and the relaxation times τ (Figure 3d). The distribution of these relaxation times is α = 0.383±0.052, suggesting multiple relaxation pathways. We therefore analysed the data shown in the Arrhenius plot considering numerous slow relaxation processes and found an adequate description by adopting Orbach, Raman and direct relaxation processes. The corresponding formula is given by $\tau^{-1} = \tau_0^{-1}\exp(-U_{eff}/k_BT) + CT^n + A_KT$ (k_B: Boltzmann's constant). The least-squares fit yields an attempt time τ_0 = (1.08±0.31)×10^{-7} s and an effective barrier U_{eff} = (33.7±1.5) cm^{-1} for the Orbach process, a constant C = (0.41±0.08) s^{-1}K^{-n} and an exponent n = 4.9±0.2 for the Raman process, and a constant A_K = (8.9±0.6) s^{-1}K^{-1} at 500 Oe static bias field for the direct process. The Orbach process parameters are in the common range of Dy^{III} SIMs,[10] while the parameters for the Raman and direct processes are within the expected range for systems with closely spaced Kramers levels (n = 5).[55] The corresponding homoleptic double-decker complexes, *i.e.* $[Dy^{III}(Pc)_2]^-$ and $[Dy^{III}(PW_{11}O_{39})_2]^{11-}$, exhibit effective energy barriers U_{eff} = 28 and 38.2 cm^{-1} and τ_0 values of 6.25 × 10^{-6} and 9.6× 10^{-12} s respectively.[15,56] The U_{eff} value of **2** thus represents the average value, however, in contrast to $[Dy^{III}(PW_{11}O_{39})_2]^{11-}$, it shows a more pronounced curvature of the isotherms in the Cole-Cole plot (at a significantly smaller bias field; 500 Oe *vs.* 3000 Oe).

In conclusion, we have reported the synthesis and characterisation of a family of new hybrid complexes of formula $[M^{III}(Pc)(PW_{11}O_{39})]^{6-}$, formed by combining two tetradentate ligands with donor atoms forming O_4 and N_4 squares of nearly identical size (ca. 2.8 Å side length), namely the polyoxotungstate $[PW_{11}O_{39}]^{7-}$ and unsubstituted phthalocyanate. The observation of SMM behaviour in **2** will prompt further investigations into the derivatisation of the peripheral hydrogens on the Pc ligand (*e.g.* with electron-donating and electron-withdrawing groups) and the use of other lacunary POMs (Keggin and Wells-Dawson type) to study the magnetic response.

Conflicts of interest

There are no conflicts to declare.

Notes and references

Crystal Data. 3: $C_{76}H_{122}N_{12}O_{39}PW_{11}Tb{\cdot}6(CH_2Cl_2)$ M_r = 4549.64 g mol^{-1}, monoclinic, *C*2/*m* (No. 12), a = 22.5917(14) Å, b = 21.7413(12) Å, c = 26.2648(15) Å, β = 95.3550(10)°, $\alpha = \gamma$ = 90°, V = 12844.3(13) Å^3, T = 100.15 K, Z = 4, Z' = 0.5, μ(Synchrotron) = 9.767, 53920 reflections measured, 7102 unique (R_{int} = 0.0833) which were used in all calculations. The final wR_2 was 0.1507 (all data) and R_1 was 0.0509 (I > 2(I)). CCDC number: 1993275.

1: $C_{192}H_{324}N_{24}O_{78}P_2W_{22}Y{\cdot}3.5(CH_2Cl_2)$, M_r = 8798.43 g mol^{-1}, monoclinic, $P2_1/c$ (No. 14), a = 29.676(4) Å, b = 30.709(4) Å, c = 29.725(4) Å, β = 91.830(2)°, $\alpha = \gamma$ = 90°, V = 27074(5) Å^3, T = 100.0 K, Z = 4, Z' = 1, μ(Synchrotron) = 9.036, 213327 reflections measured, 28548 unique (R_{int} = 0.1538) which were used in all calculations. The final wR_2 was 0.2344 (all data) and R_1 was 0.0869 (I > 2(I)). CCDC number: 1993274.

We thank the Punjab Educational Endowment Fund (PEEF) for Ms. Sidra Sarwar's CMMS Scholarship.

1. G. Christou, D. Gatteschi, D. N. Hendrickson and R. Sessoli, *MRS Bull.*, 2000, **25**, 66.
2. R. Sessoli, D. Gatteschi, A. Caneschi and M. Novak, *Nature*, 1993, **365**, 141.
3. L. Bogani and W. Wernsdorfer, *Nat. Mater.*, 2008, **7**, 179.
4. K. Katoh, H. Isshiki, T. Komeda and M. Yamashita, *Chem. Asian J.*, 2012, **7**, 1154.

5. K. Katoh, H. Isshiki, T. Komeda and M. Yamashita, *Coord. Chem. Rev.*, 2011, **255**, 2124.
6. E. Moreno-Pineda, C. Godfrin, F. Balestro, W. Wernsdorfer and M. Ruben, *Chem. Soc. Rev.*, 2018, **47**, 501.
7. A. Gaita-Ariño, F. Luis, S. Hill and E. Coronado, *Nat. Chem.*, 2019, **11**, 301.
8. M. Urdampilleta, N.-V. Nguyen, J.-P. Cleuziou, S. Klyatskaya, M. Ruben and W. Wernsdorfer, *Int. J. Mol. Sci.*, 2011, **12**, 6656.
9. N. Ishikawa, M. Sugita and W. Wernsdorfer, *J. Am. Chem. Soc.*, 2005, **127**, 3650.
10. D. N. Woodruff, R. E. P. Winpenny and R. A. Layfield, *Chem. Rev.*, 2013, **113**, 5110.
11. J. Luzon and R. Sessoli, *Dalton Trans.*, 2012, **41**, 13556.
12. J. D. Rinehart and J. R. Long, *Chem. Sci.*, 2011, **2**, 2078.
13. S. T. Liddle and J. van Slageren, *Chem. Soc. Rev.*, 2015, **44**, 6655.
14. J.-L. Liu, Y.-C. Chen and M.-L. Tong, *Chem. Soc. Rev.*, 2018, **47**, 2431.
15. N. Ishikawa, M. Sugita, T. Ishikawa, S.-Y. Koshihara and Y. Kaizu, *J. Am. Chem. Soc.*, 2003, **125**, 8694.
16. S.-D. Jiang, B.-W. Wang, H.-L. Sun, Z.-M. Wang and S. Gao, *J. Am. Chem. Soc.*, 2011, **133**, 4730.
17. S. D. Jiang, B. W. Wang, G. Su, Z. M. Wang and S. Gao, *Angew. Chem., Int. Ed.*, 2010, **49**, 7448.
18. L. Ungur, J. J. Le Roy, I. Korobkov, M. Murugesu and L. F. Chibotaru, *Angew. Chem., Int. Ed.,* 2014, **53**, 4413.
19. M. Gonidec, F. Luis, À. Vílchez, J. Esquena, D. B. Amabilino and J. Veciana, *Angew. Chem., Int. Ed.*, 2010, **49**, 1623.
20. C. R. Ganivet, B. Ballesteros, G. de la Torre, J. M. Clemente-Juan, E. Coronado and T. Torres, *Chem. Eur. J.*, 2013, **19**, 1457.
21. M. Gonidec, I. Krivokapic, J. Vidal-Gancedo, E. S. Davies, J. McMaster, S. M. Gorun and J. Veciana, *Inorg. Chem.*, 2013, **52**, 4464.
22. H. Shang, S. Zeng, H. Wang, J. Dou and J. Jiang, *Sci. Rep.*, 2015, **5**, 8838.
23. M. Gonidec, D. B. Amabilino and J. Veciana, *Dalton Trans.*, 2012, **41**, 13632.
24. Y. Chen, F. Ma, X. Chen, B. Dong, K. Wang, S. Jiang, C. Wang, X. Chen, D. Qi and H. Sun, *Inorg. Chem. Front.*, 2017, **4**, 1465.
25. Y. Chen, F. Ma, X. Chen, B. Dong, K. Wang, S. Jiang, C. Wang, X. Chen, D. Qi and H. Sun, *Inorg. Chem.*, 2017, **56**, 13889.
26. F. Gao, Y.-Y. Li, C.-M. Liu, Y.-Z. Li and J.-L. Zuo, *Dalton Trans.*, 2013, **42**, 11043.
27. H. Ke, W. K. Wong, W. Y. Wong, H. L. Tam, C. T. Poon and F. Jiang, *Eur. J. Inorg. Chem.*, 2009, **2009**, 1243.
28. F. Lu, X. Sun, R. Li, D. Liang, P. Zhu, C.-F. Choi, D. K. Ng, T. Fukuda, N. Kobayashi and M. Bai, *New. J. Chem.*, 2004, **28**, 1116.
29. F. Gao, X. Feng, L. Yang and X. Chen, *Dalton Trans*, 2016, **45**, 7476.
30. G. Lu, S. Yan, M. Shi, W. Yu, J. Li, W. Zhu, Z. Ou and K. M. Kadish, *Chem. Commun.*, 2015, **51**, 2411.
31. H. Wang, K. Wang, J. Tao and J. Jiang, *Chem. Commun.*, 2012, **48**, 2973.
32. W. Cao, Y. Zhang, H. Wang, K. Wang and J. Jiang, *RSC Adv.*, 2015, **5**, 17732.
33. H. Wang, W. Cao, T. Liu, C. Duan and J. Jiang, *Chem. Eur. J.*, 2013, **19**, 2266.
34. W. Cao, C. Gao, Y.-Q. Zhang, D. Qi, T. Liu, K. Wang, C. Duan, S. Gao and J. Jiang, *Chem. Sci.*, 2015, **6**, 5947.
35. E. Coronado and C. J. Gomez-Garcia, *Chem. Rev.*, 1998, **98**, 273.
36. L. Ruhlmann and D. Schaming, *Trends in Polyoxometalates Research*, Nova Science Publishers, New York, 2015.
37. N. V. Izarova and P. Kögerler, in *Trends in Polyoxometalates Research*, ed. L. Ruhlmann and D. Schaming, Nova Science Publishers, New York, 2015, pp. 121-149.
38. Y.-F. Song, *Polyoxometalate-Based Assemblies and Functional Materials*, Springer International Publishing, 2018.
39. S.-S. Wang and G.-Y. Yang, *Chem. Rev.*, 2015, **115**, 4893.
40. K. Y. Monakhov, M. Moors and P. Kögerler, in *Advances in Inorganic Chem*istry, ed. R. van Eldik and L. Cronin, Academic Press, Elsevier, Amsterdam, 2017, vol. 69, pp. 251-286.
41. J.-P. Wang, J.-W. Zhao, X.-Y. Duan and J.-Y. Niu, *Cryst. Growth Des.*, 2006, **6**, 507.
42. S. Zhang, Y. Wang, J. Zhao, P. Ma, J. Wang and J. Niu, *Dalton Trans.*, 2012, **41**, 3764.
43. K. Wang, D. Zhang, J. Ma, P. Ma, J. Niu and J. Wang, *CrystEngComm*, 2012, **14**, 3205.
44. H.-Y. Zhao, J.-W. Zhao, B.-F. Yang, H. He and G.-Y. Yang, *CrystEngComm*, 2013, **15**, 8186.
45. J. Iijima, H. Naruke and T. Sanji, *RSC Adv.*, 2016, **6**, 91494.
46. R. Pütt, X. Qiu, P. Kozłowski, H. Gildenast, O. Linnenberg, S. Zahn, R. Chiechi and K. Monakhov, *Chem. Commun.*, 2019, **55**, 13554.
47. Y. Bian, R. Wang, D. Wang, P. Zhu, R. Li, J. Dou, W. Liu, C.-F. Choi, H.-S. Chan, C. Ma, D. K. P. Ng and J. Jiang, *Helv. Chim. Acta.*, 2004, **87**, 2581.
48. M. M. Ayhan, A. Singh, E. Jeanneau, V. Ahsen, J. Zyss, I. Ledoux-Rak, A. G. Gürek, C. Hirel, Y. Bretonnière and C. Andraud, *Inorg. Chem.*, 2014, **53**, 4359.
49. V. E. Pushkarev, V. V. Kalashnikov, A. Y. Tolbin, S. A. Trashin, N. E. Borisova, S. V. Simonov, V. B. Rybakov, L. G. Tomilova and N. S. Zefirov, *Dalton Trans.*, 2015, **44**, 16553.
50. P. Zhu, F. Lu, N. Pan, Dennis P. Arnold, S. Zhang and J. Jiang, *Eur. J. Inorg. Chem.*, 2004, **2004**, 510.
51. M. Arıcı, C. Bozoğlu, A. Erdoğmuş, A. L. Uğur and A. Koca, *Electrochim. Acta.*, 2013, **113**, 668.
52. E. B. Orman, A. Koca, A. R. Özkaya, İ. Gürol, M. Durmuş and V. Ahsen, *J. Electrochem. Soc.*, 2014, **161**, H422.
53. H. Lueken, *Magnetochemie*, Teubner, Stuttgart, 1999.
54. K. S. Cole and R. H. Cole, *J. Chem. Phys.*, 1941, **9**, 341.
55. K. N. Shrivastava, Phys. Stat. Sol. B, 1983, **117**, 437.
56. P. Ma, F. Hu, Y. Huo, D. Zhang, C. Zhang, J. Niu and J. Wang, *Cryst. Growth Des.*, 2017, **17**, 1947.

